Image dehazing based on partitioning reconstruction and entropy-based alternating fast-weighted guided filters

Yuanyu Wang[a] and Peter Yuen[b,*]
[a]Taiyuan University of Technology, School of Computer Science and Technology, Jinzhong, China
[b]Cranfield University, Defence Academy of UK, Shrivenham, United Kingdom

Abstract. A robust image dehazing algorithm based on the first-order scattering of the image degradation model is proposed. In this work, there are three contributions toward image dehazing: (i) a robust method for assessing the global irradiance from the most hazy-opaque regions of the imagery is proposed; (ii) more detailed depth information of the scene can be recovered through the enhancement of the transmission map using scene partitions and entropy-based alternating fast-weighted guided filters; and (iii) crucial model parameters are extracted from in-scene information. This paper briefly outlines the principle of the proposed technique and compares the dehazed results with four other dehazing algorithms using a variety of different types of imageries. The dehazed images have been assessed through a quality figure-of-merit, and experiments have shown that the proposed algorithm effectively removes haze and has achieved a much better quality of dehazed images than all other state-of-the-art dehazing methods employed in this work. © *2017 Society of Photo-Optical Instrumentation Engineers (SPIE)* [DOI: 10.1117/1.OE.56.5.053111]

Keywords: image dehazing; partitioning reconstruction; alternating fast-weighted guided filters; transmission.

Paper 170432 received Mar. 22, 2017; accepted for publication May 8, 2017; published online May 26, 2017.

1 Introduction

Haze removal from a single image is a challenging problem, especially when depth information of the imagery is not available. State-of-the-art techniques for dehazing single image data can be roughly classified into two schemes. The first approach is based on image enhancements that aim at improving the visual quality of the image through denoising and midtone compression, such as histogram equalization,[1] local contrast maximization-based technique[2] color constancy Retinex approach,[3] fusion-based,[4] and fuzzy set enhancements.[5] These techniques attempted to resolve the problem but without any measures to address the source of image degradation; consequently, these methods could not improve the contrast and the visibility of the hazy scene sufficiently. The second scheme is based on priors or assumptions to help model the statistics of the scattering event, thereby solving the ill-posed inverse problem of haze removal. Fattal[6] proposed a dehazing method under the assumption that the scattering of light by objects in the scene and the surface shading are locally statistically uncorrelated. Tarel et al.[7] imposed constraints on the variation of the depth by maximizing the atmospheric veil (AVM), assuming that it must be smooth for most of the time. He et al.[8] explored the dark channel prior (DCP) based on the statistics of haze-free images. The DCP had been widely used in bad weather image restoration.[9–12] Meng et al.[13] proposed an effective regularization dehazing method to obtain a haze-free image by exploring the inherent boundary constraint (BCR). Zhu et al.[14] proposed the color attenuation prior (CAP) by creating a linear model for dehazing the image. Although these haze-relevant priors or assumptions have some success for dehazing images, they are not really effective or efficient enough, and at times unwanted artifacts have been seen in the results produced by these dehazing approaches.

In this paper, a physics-based algorithm within the image degradation model using partitioning reconstruction and alternating fast-weighted guided filters (FWGFs) is proposed for more robust dehazing of a single image. The proposed method first finds the mostly haze-opaque region (MHOR) from the hazy image. Then the global irradiance is estimated from the MHOR of the scene. The depth of the scene is estimated through a transmission map reconstructed by transmission partitions from the haze-free slices of the image. The transmission map is subsequently refined by an entropy-based alternating FWGF to reduce residual halo artifacts in the restored image. The quality of the dehazed images is assessed through a quality figure-of-merit (FOM) to evaluate the effectiveness of the dehazing algorithm. The robustness of the proposed physics-based approach is compared with four other state-of-the-art dehazing methods, and experiments have shown superior qualities of dehazed results obtained from this work.

2 Proposed Algorithm

2.1 *Haze Image Degradation Model*

The present image restoration work is based on the image degradation model with first order multiple scattering:

$$I^c = J^c e^{-\tau}\left[1+\frac{p(0,0)}{4\pi}\tau\right]+A^c(1-e^{-\tau}), c\in\{r,g,b\}, \quad (1)$$

where I^c is the hazy input image, J^c is the intrinsic haze-free image of the scene, $\tau \in [0.8,1]$ is the visibility,[15] A^c is the global irradiance, p is phase function, and $p(0, 0)$ is the

*Address all correspondence to: Peter Yuen, E-mail: p.yuen@cranfield.ac.uk

0091-3286/2017/$25.00 © 2017 SPIE

Downloaded From: http://opticalengineering.spiedigitallibrary.org/ on 07/03/2017 Terms of Use: http://spiedigitallibrary.org/ss/termsofuse.aspx

phase function of a single haze particle, which can be evaluated under the spherical Lambertian scattering assumption.[16] Let $t = e^{-\tau}$ be the transmissivity and $k = 1 + [p(0,0)\tau]/(4\pi)$ be the scattering phase factor, which can be treated as a constant for a given scene.[17] The value of k can be calculated according to Ref. 17. Then, we can transform Eq. (1) into

$$J^c = \frac{I^c - A^c(1-t)}{tk}. \tag{2}$$

Thus, J^c can be recovered from Eq. (2) when A^c, t, and k are known.

2.2 *Global Irradiance Estimation*

In most cases, the global irradiance can be estimated from the MHOR of the scene.[18–20] However, previous work in the area failed to locate the MHOR robustly due to the false alarms given by the white or bright pixels in the imagery. The present work constrains the search of MHOR by selecting chromatically whitish pixels, particularly in the upper part of the imagery, which, in many cases, represents the pixels of the direct skylight.

A white balancing algorithm for chromatic balance is then applied for the whole scene before A^c is estimated through the matrix R:

$$R = 1 - \left(\max_{c\in\{r,g,b\}} I^c - \min_{c\in\{r,g,b\}} I^c \right). \tag{3}$$

Then, a selective operator S for the selection of chromatically whitish pixels:

$$S \to R_{I_g < \bar{I}_g} = 0, \tag{4}$$

where $\bar{I}_g$ is the mean of all grayscale pixels in I^c and I_g is the chromatic values of each pixel. Because MHOR usually lies at the top part of the haze image, the MHOR is selected via a spatially weighted matrix W:

$$W = 1 - [(i/N)', \ldots, (i/N)'], \quad i \in \{1, \ldots, N\}, \tag{5}$$

where N is the row numbers of the image. A minimum filter is then applied to exclude outlier pixels, such as bright noise. A soft threshold T_R is then defined for the selection of MHOR:

$$T_R = \rho \cdot \max\{[W \cdot S(R)] * f\}, \tag{6}$$

where f is a min filter, * is the convolution operator, and ρ is the percentage of the brightest pixel, which is used to adjust the value of T_R; it is a constant between 0 and 1, and $\rho = 0.99$ has been used here. Finally, A^c can be obtained by averaging MHOR in the I^c:

$$A^c = \overline{\{I^c_{\Omega\in[W\cdot S(R)]*f>T_R}\}}, \tag{7}$$

where Ω represents the MHOR with all pixels above T_R.

2.3 *Transmission Estimation*

For a given A^c, the J^c can be expressed in a unary function of t as in Eq. (2). A series of J^c_1 to J^c_n slices can be generated for a range of t that varies from t_1 to t_n. Haze-free regions of each slice can be found through a detection operator. Ancuti et al.[4] proposed a similar detection-based method for image dehazing. However, this method is not robust and suffers from large error due to the ambiguity in assessing the color and depth correctly. The proposed method in this paper is shown to be capable of reducing this color/depth ambiguity by an automatic pace and a nonoverlapped haze-free areas selection, as well as a better algorithm for the detection of the haze-free region.

Our detection operator D is effectively the process of Eq. (8) to Eq. (10), as illustrated below:

Unlike Ref. 4, the semi-inverse image can be defined as follows:

$$I_s = \max(I_{\min}, 1 - I_{\min}), \quad I_{\min} = \min_{c\in\{r,g,b\}} (I^c). \tag{8}$$

The haze-free areas of the image are the regions of interest that satisfy the condition of

$$(I_s - I_{\min}) \geq H, \quad H = \min_{c\in\{r,g,b\}} (A^c). \tag{9}$$

Similar to Ref. 13, the pixels in the regions with intensities above threshold of $thL = 1 - H$ or below $thU = H$ are selected as haze-free areas in this work:

$$I_{\min} \leq thL, \quad I_{\min} \geq thU. \tag{10}$$

The process for employing Eq. (8) to Eq. (10) is collectively termed the operator D.

The haze-free area Ω in each slice i is defined as

$$\begin{cases} \Omega(J^c_i) = D(J^c_i) - \Omega(J^c_{i-1}) \\ \Omega(J^c_0) = \varnothing \end{cases}, i > 0, \tag{11}$$

where A is the null set and the depth of $\Omega(J^c_i)$ can be recovered from the transmissivity $t_i - 1$ and t_i. When $t = t_i$, the haze-free region $\Omega(J^c_i)$ represents a transmission partition of the imagery, and t_i is the transmission of the i'th partition slice. The combined transmission map of the imagery $\hat{t}$ can be reconstructed from all the transmission partitions, as shown in Eq. (12):

$$\hat{t} = \bigcup_{i=1}^{n-1} t_{i\Omega(J^c_i)} \bigcup t_{n\Omega(J^c_n) - \bigcup_{i=1}^{n-1}\Omega(J^c_i)}, \tag{12}$$

where $\cup$ is the set union and $\hat{t}$ can be constructed from $t_i = 1$ to $t_n < T$ with step length η and $T = 1 - H$. The step η has been made adaptive through an empirically developed formula, as shown in Eq. (13):

$$\eta = \frac{(1-T)}{\lfloor\{200/[\lfloor\log_{10}(M\times N)\rfloor]\}\rfloor}, \tag{13}$$

where M and N are the row and column dimensions of the image, respectively, and the bracket $\lfloor\rfloor$ is the round down operator.

2.4 *Hazy Image Restoration*

It is necessary to refine the transmission map as obtained from Eq. (12), and an FWGF is proposed to reduce halo

Downloaded From: http://opticalengineering.spiedigitallibrary.org/ on 07/03/2017 Terms of Use: http://spiedigitallibrary.org/ss/termsofuse.aspx

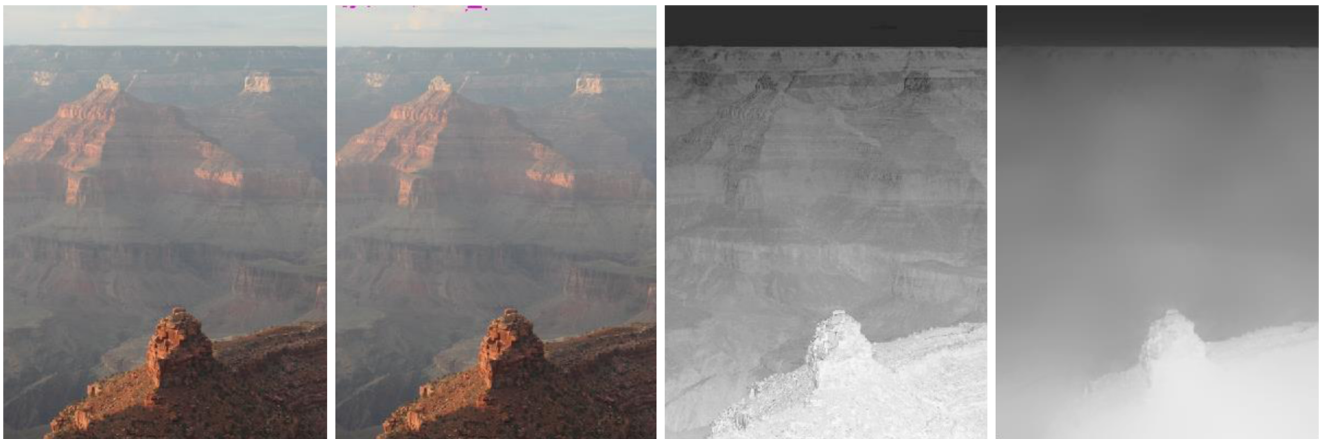


Fig. 1 (a) The proposed method for processing the hazy image and (b) the detection of the MHOR (red areas). (c) and (d) The first stage and the refined transmission map, respectively.

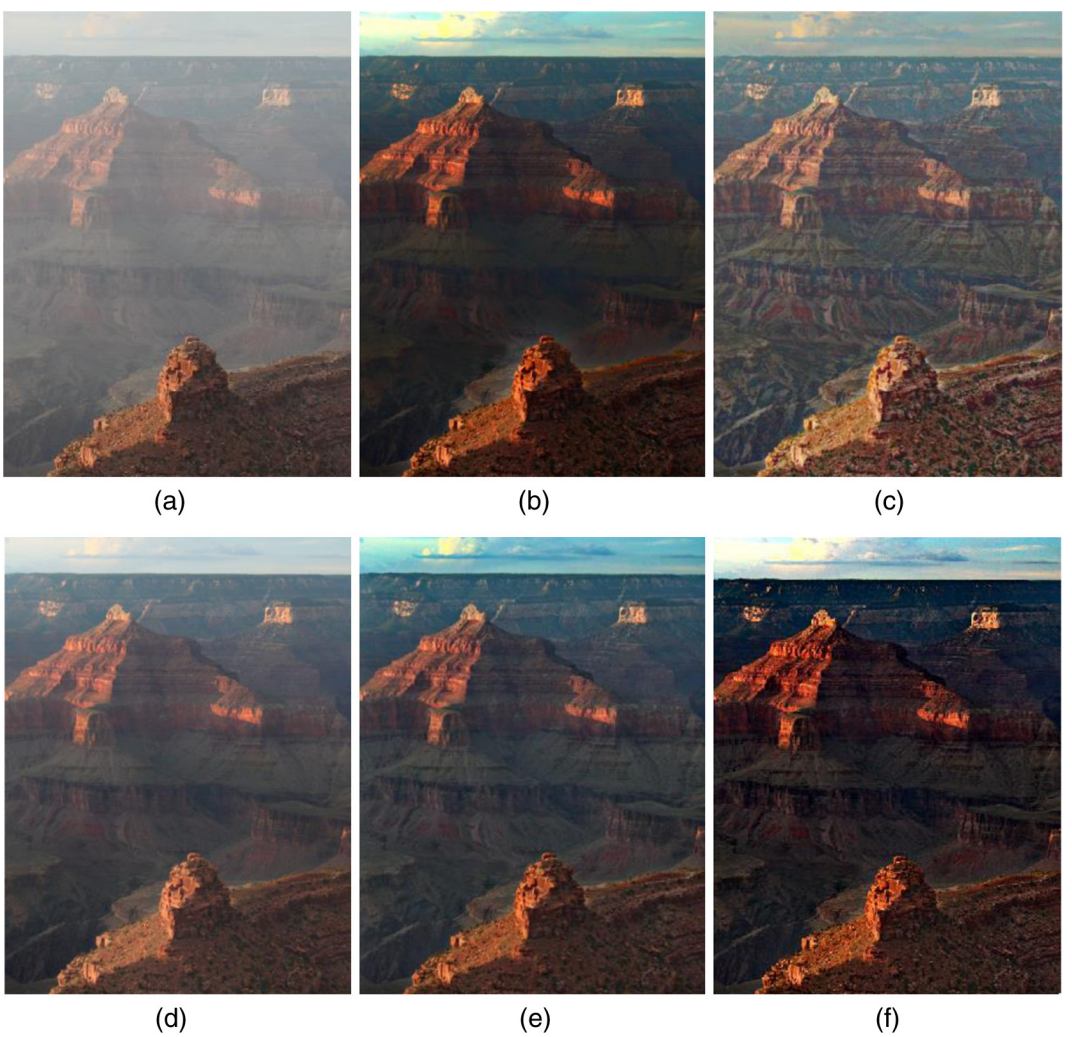


Fig. 2 The dehazed results: (a) the input hazy image 1, (b) result by DCP[8] with FOM3.42, (c) result by AVM[7] with FOM4.78, (d) result by CAP[14] with FOM3.93, (e) result by BCR[13] result with FOM3.93, and (f) the result of the proposed method with FOM5.19.

Downloaded From: http://opticalengineering.spiedigitallibrary.org/ on 07/03/2017 Terms of Use: http://spiedigitallibrary.org/ss/termsofuse.aspx

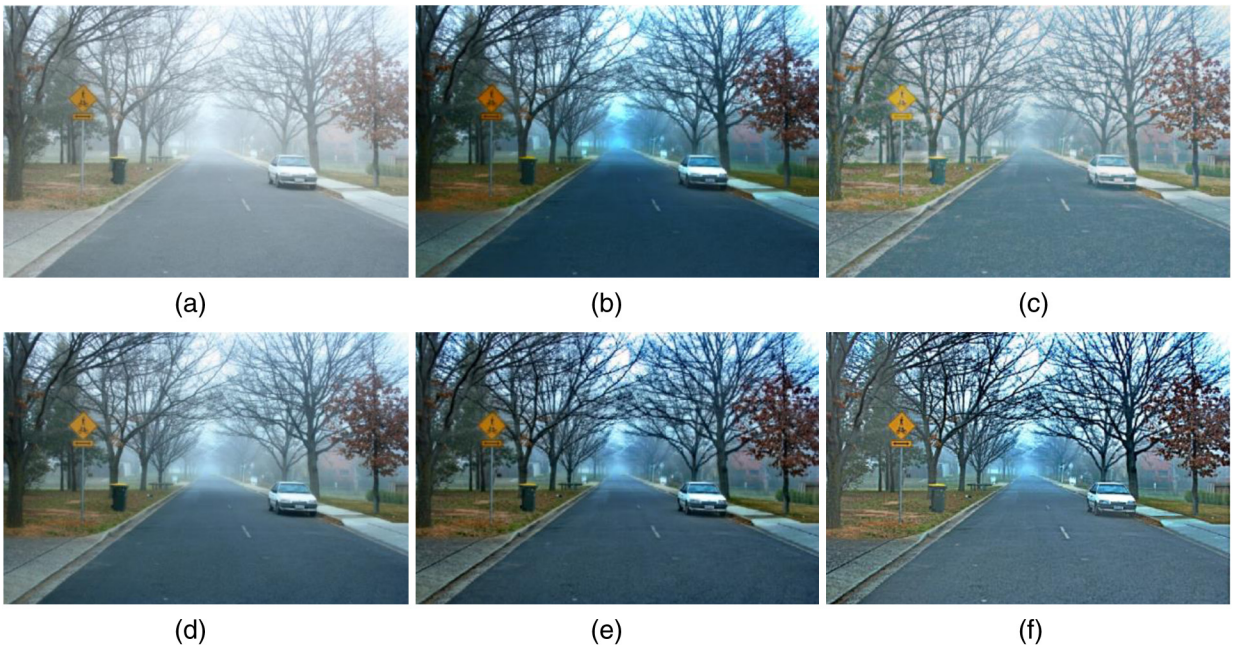


Fig. 3 The dehazed results for image 2: (a) the input hazy image 2, (b) result by processed by DCP[8] with FOM2.08, (c) result by AVM[7] with FOM2.87, (d) result by CAP[14] with FOM1.90, (e) result by BCR[13] with FOM3.14, and (f) the result by the proposed method with FOM3.52.

artifacts and roughness caused by the fixed regularization parameter in the fast guided filter.[21] A modified local variances-based and edge-sensitive weighting function, as originally proposed in Ref. 22, has been employed to incorporate local entropy for enhancing the transmission map. The weighting function W_G is defined as

$$W_G(p') = \frac{1}{N}\sum_{p=1}^{N}\frac{E_G(p')+\lambda}{E_G(p)+\lambda}, \tag{14}$$

where E_G is the image entropy of the guidance image G in a 3×3 window, p is a pixel in the window, and p' is the center

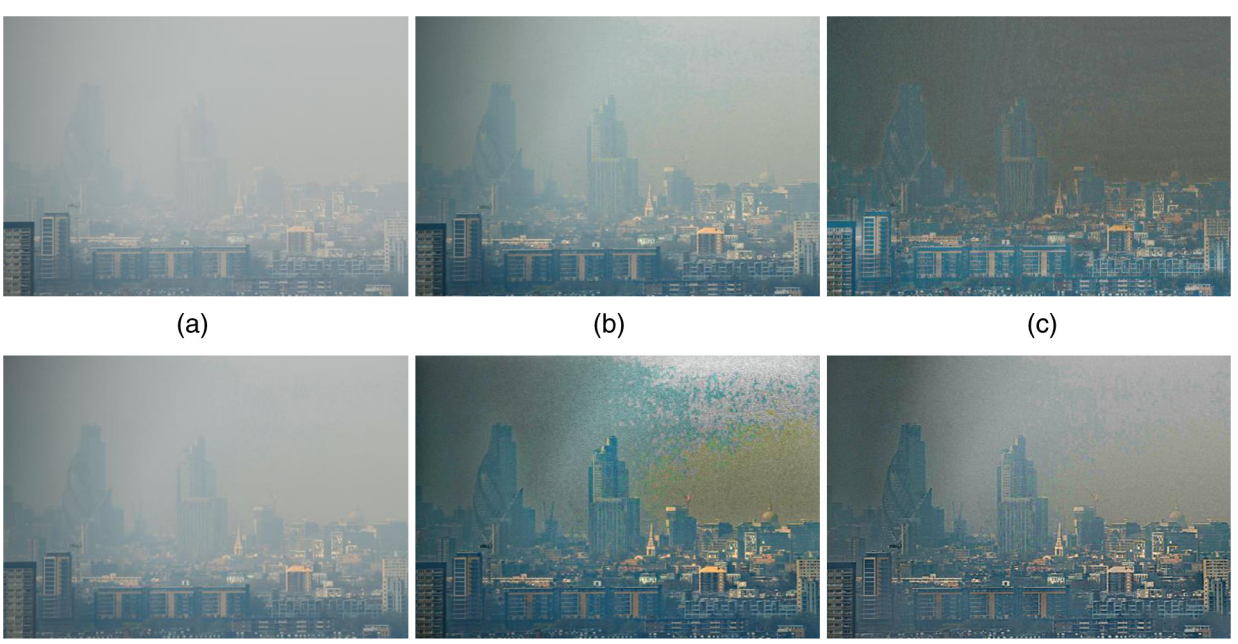


Fig. 4 The dehazed results for image 3: (a) the input hazy image, (b) result by DCP[8] with FOM2.34, (c) result by AVM[7] with FOM5.00, (d) result by CAP[14] with FOM1.59, (e) result by BCR[13] with FOM5.79, and (f) the result obtained by the proposed method with FOM6.18.

Downloaded From: http://opticalengineering.spiedigitallibrary.org/ on 07/03/2017 Terms of Use: http://spiedigitallibrary.org/ss/termsofuse.aspx

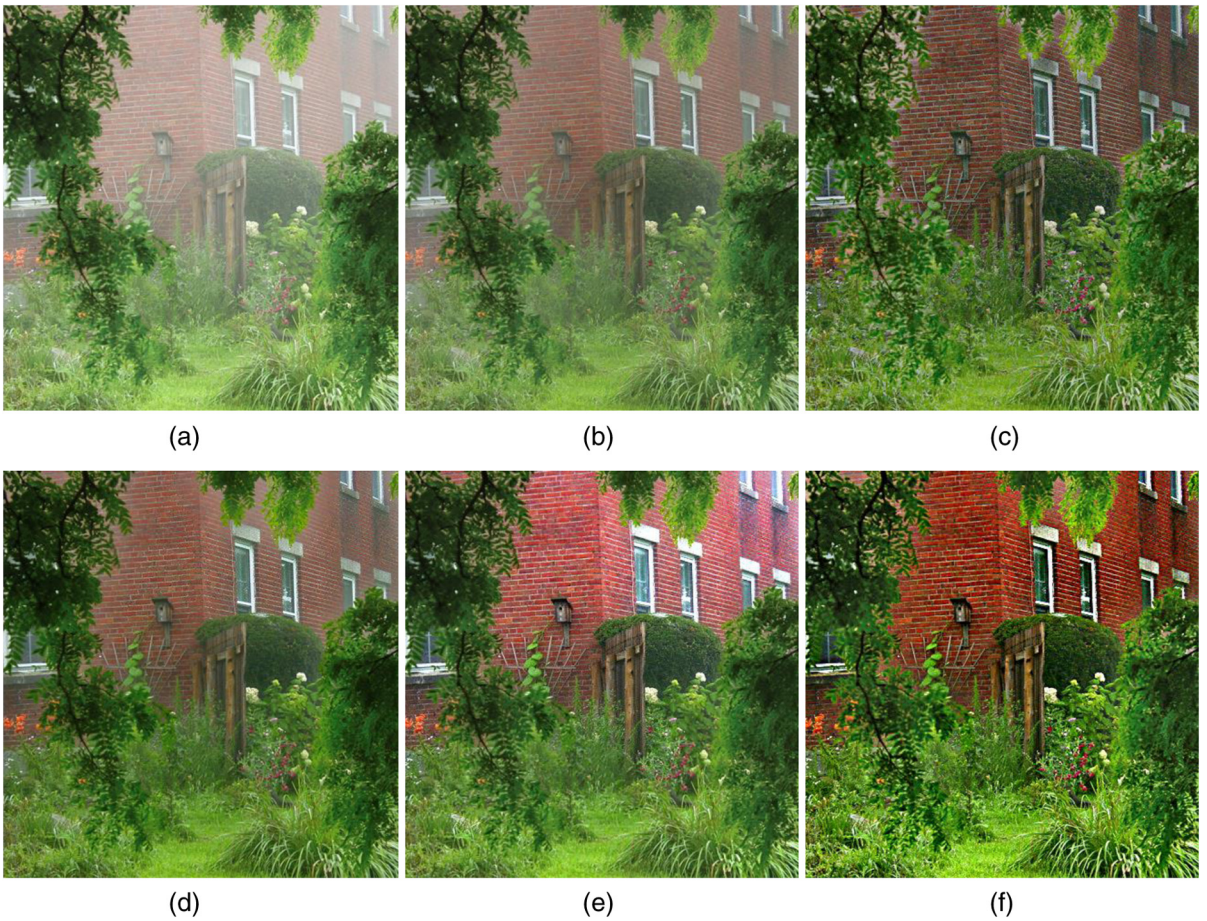


Fig. 5 The dehazed results for image 4: (a) the input hazy image, (b) result by DCP[8] with FOM1.69, (c) result by AVM[7] with FOM2.43, (d) result by CAP[14] with FOM1.58, (e) result by BCR[13] with FOM2.33, and (f) the result obtained by the proposed method with FOM2.94.



Fig. 6 The dehazed results for image 5: (a) the input hazy image, (b) result by DCP[8] with FOM1.73, (c) result by AVM[7] with FOM2.41, (d) result by CAP[14] with FOM1.48, (e) result by BCR[13] with FOM2.02, and (f) the result obtained by the proposed method with FOM3.19.

Downloaded From: http://opticalengineering.spiedigitallibrary.org/ on 07/03/2017 Terms of Use: http://spiedigitallibrary.org/ss/termsofuse.aspx

pixel. In this paper, λ is 0.001 times the dynamic range of the input image. Then, the linear coefficients a_k and b_k of the FWGF can be obtained:

$$a_k = \left(\frac{1}{|\omega|}\sum_{i\in\omega_k} G_i q_i - \mu_k \bar{q_k}\right) / \left(\sigma_k^2 + \frac{0.001}{W_G}\right) \downarrow, \tag{15}$$

$$b_k = \bar{q_k} - a_k \mu_k, \bar{q_k} = \frac{1}{|\omega|}\sum_{i\in\omega_k} q_i \downarrow, \tag{16}$$

where ω_k is square window of radius r, (note: r is the radius of the boxfilter, which is used as a moving sum filter. The size of the boxfilter is $2r$.) $|\omega|$ is the number of pixels in ω_k, μ_k and σ_k^2 are the mean and variance of ω_k in the transmission map $\hat{t}$, respectively, and q_k are pixels in ω_k. The G, $\hat{t}$, and W_G in Eq. (15) to Eq. (16) have been down subsampled $\downarrow$ by a subsampling ratio s for better computational efficiency. The output O is obtained by upsampling $\uparrow$ through the averages of a_k and b_k:

$$O_i = \frac{1}{|\omega|}\sum_{k|i\in\omega_k} (a_k G_k + b_k) \uparrow . \tag{17}$$

To further improve the algorithm, FWGF within the alternating guided filter (AGF) framework[23] is proposed. The AGF consists of two FWGFs. For a given G_0 as the initial guided image, the FWGF employed in this work has adopted $r = 20$ and $s = 4$, as suggested in Ref. 21 for better computational efficiency. The pseudocode for the alternating FWGF with t as the refined transmission map is summarized as follows:

Initialize $G_0 = 0$
do
$G_i \leftarrow \text{FWGF}(G_{i-1}, \hat{t}, r, s)$
$G_i \leftarrow \text{FWGF}(\hat{t}, G_i, r, s)$
until $G_i - G_{i-1} < 0.01$
$t = Gi$.

The algorithm converges fast normally within a few iterations, and it terminates when $G_i - G_{i-1}$ is less than 0.01. The intrinsic image J^c can be evaluated as in Eq. (2). However, the phase factor k reduces the chromatic intensity of pixels and contrast due to scattering. Thus, an adaptive contrast enhancement algorithm[24] is applied to overcome this problem.

3 Experimental Results

Experiments have been carried out on a Lenova-Y40-80 2.40GHz Core i7-5500U laptop under MATLAB (R2015b). Various types of imagery have been processed using several state-of-the-art dehazing algorithms, and the dehazed results have been compared with those obtained by the proposed method. Three metrics of image quality assessments (IQAs) have been adopted to evaluate the effectiveness of the dehazing algorithm: the indicator X_e represents the rate of visible edges with respected to the input image, X_r indicates the quality of the contrast[25] with respect to that of the input hazy image, and X_o is the standard deviation of the dehazed image. A high quality dehazed result is characterized by high values of X_e, X_r, and X_o. A combination of these three scores into a FOM $= X_e + X_r + X_o$ is constructed for quality assessment of image dehazing. This FOM is designed to evaluate the recovery of the haze features through the X_e and X_r metrics, as originally proposed in Ref. 25, and to include the X_o, which is traditionally employed for measuring image contrast. Thus, the proposed FOM is sensitive to the amplified background noise and blocking artifacts.[26] In addition, the computational complexity of all algorithms is compared in terms of processing time T_c (in seconds).

Figures 1(a) and 1(b) show the hazy input image and the MHOR as located by the proposed method. Figures 1(c) and 1(d) depict the transmission map and the refined transmission map after processed by algorithms, as described in Secs. 2.3 and 2.4.

Table 1 Quantitative assessment of dehazed output images processed by various algorithms.

Test	Methods	X_e	X_r	X_o	FOM	T_c(s)
Image 1	DCP[8]	1.86	1.25	0.31	3.42	123.2
	AVM[7]	2.11	2.29	0.37	4.78	8.5
	CAP[14]	1.09	1.19	0.34	2.64	8.3
	BCR[13]	1.85	1.76	0.31	3.93	4.8
	Proposed	2.20	2.66	0.31	5.19	2.5
Image 2	DCP[8]	0.30	1.58	0.20	2.08	100.3
	AVM[7]	0.54	2.16	0.16	2.87	7.6
	CAP[14]	0.32	1.37	0.20	1.90	4.3
	BCR[13]	0.50	2.43	0.20	3.14	3.8
	Proposed	0.56	2.78	0.17	3.52	1.9
Image 3	DCP[8]	0.47	1.75	0.12	2.34	237.5
	AVM[7]	1.24	3.68	0.06	5.00	32.3
	CAP[14]	0.19	1.28	0.11	1.59	8.0
	BCR[13]	1.58	4.06	0.14	5.79	6.6
	Proposed	1.39	4.71	0.07	6.18	5.1
Image 4	DCP[8]	0.12	1.22	0.34	1.69	91.7
	AVM[7]	0.25	1.81	0.36	2.43	4.1
	CAP[14]	0.08	1.04	0.44	1.58	3.6
	BCR[13]	0.15	1.74	0.43	2.33	3.2
	Proposed	0.09	2.37	0.47	2.94	1.1
Image 5	DCP[8]	0.15	1.15	0.42	1.73	201.9
	AVM[7]	0.47	1.45	0.47	2.41	6.6
	CAP[14]	0.03	0.94	0.49	1.48	6.2
	BCR[13]	0.21	1.36	0.43	2.01	5.2
	Proposed	0.19	2.67	0.32	3.19	3.3

Downloaded From: http://opticalengineering.spiedigitallibrary.org/ on 07/03/2017 Terms of Use: http://spiedigitallibrary.org/ss/termsofuse.aspx

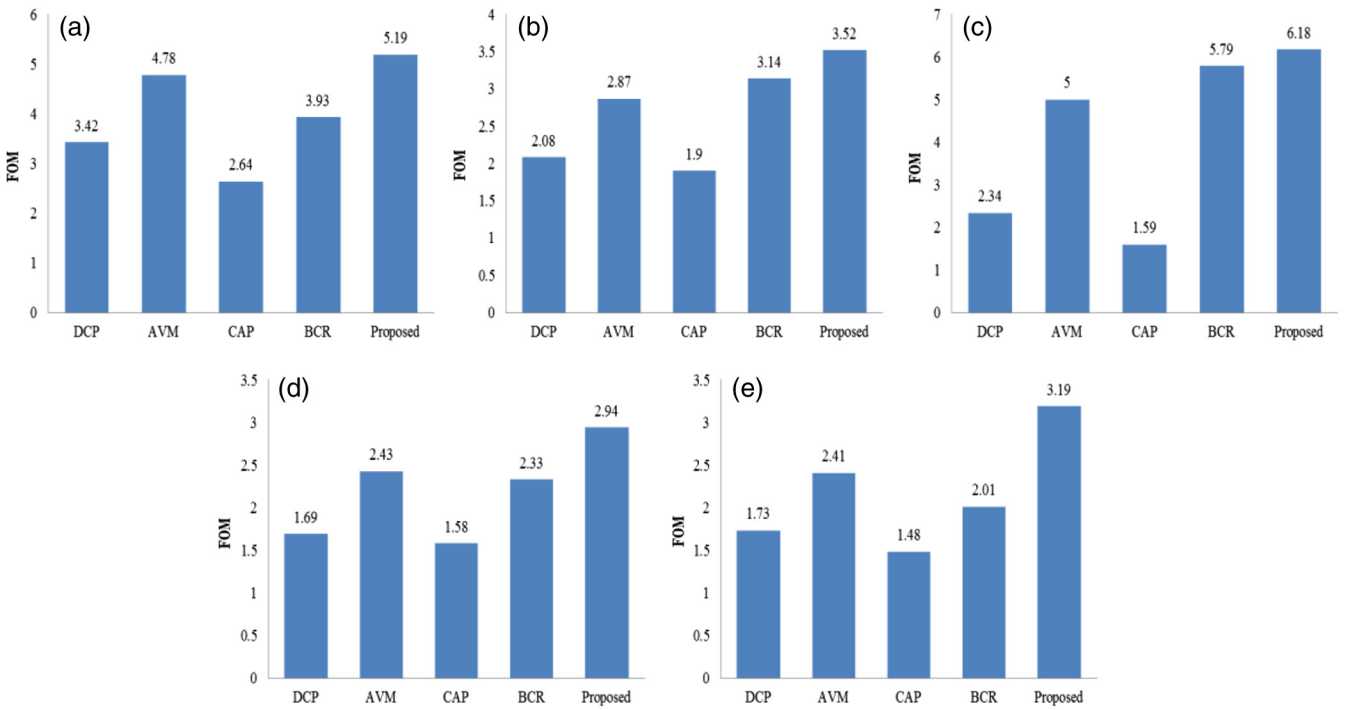


Fig. 7 The IQA for all the dehazing methods employed in this work: (a) image 1, (b) image 2, (c) image 3, (d) image 4, and (e) image 5.

We have presented the results of five hazy images processed by four state-of-the-art methods (DCP,[8] AVM,[7] CAP,[14] and BCR[13]) and compared them with the results obtained by the proposed algorithm in Figs. 2–6. The five selected images for algorithm testing in this experiment have been (i) far-view mountainous scene (image 1), (ii) near-view street scene (image 2), (iii) far-view city scene (image 3), (iv) near-view village background without the view of the sky (image 4), and (v) near field of view of a park scene (image 5). It is seen from these experimental results that the BCR method proposed by Meng et al.[13] has been the best dehazing algorithm among the 4, with FOM values very close to that of the proposed physics-based dehazing technique. However, the BCR algorithm shows a lack of robustness, and the dehazed results at times exhibit halo artifacts, as depicted in Fig. 4(c). The AVM technique also suffers from lack of depth details, which can be seen from Figs. 2 and 4. It can be observed that the proposed method improves visibility and restores contrast with a minimum of halo and block artifacts, and the proposed method works equally well for imagery that does not contain the sky view. Table 1 tabulates the FOM scores of sample images processed by all algorithms; it is shown that the quality of dehazed images that were processed by the proposed algorithm have achieved good quality with the best FOM score. A summary of the IQA for all the dehazing methods employed in this work is graphically presented in Fig. 7.

4 Conclusion

A single-image dehazing algorithm based on partitioning reconstruction and alternating FWGFs is proposed. The principle of the algorithm is to deduce the intrinsic image by assessing the global irradiance and the transmission map of the scene within the image degradation model. It is shown that the proposed algorithm is able to estimate the global irradiance more accurately through a robust detection of the MHORs from the scene even when the imagery does not contain the sky region. The depth information of the imagery is obtained through a boundary constraint transmission map of haze-free areas. The transmission map is further refined by alternating FWGFs, and the final dehazed output is obtained through the first-order multiple scattering of the image degradation model. Unlike most work in the area, the proposed method does not need prior knowledge of the statistical properties of the scene. Experiments have shown that the proposed method can significantly improve the image quality in a timely manner better than all dehazing algorithms utilized in this work.

Acknowledgments

We would like to thank our colleagues for their constructive suggestions. This work was supported by the Natural Science Foundation of Shanxi Province under Grant No. 2012011014-2.

References

1. Z. Xu, X. Liu, and X. Chen, "Fog removal from video sequences using contrast limited adaptive histogram equalization," in *Proc. IEEE Conf. Computational Intelligence and Software Engineering (CiSE 2009)*, pp. 1–4, IEEE Computer Society, Washington, DC (2009).
2. R. T. Tan, "Visibility in bad weather from a single image," in *Proc. IEEE Conf. Computing Visual Pattern Recognition (CVPR 2008)*, pp. 1–8, IEEE Computer Society, Washington, DC (2008).
3. X. Fu et al., "A novel retinex based approach for image enhancement with illumination adjustment," in *Proc. IEEE Int. Conf. Acoustics, Speech, and Signal Processing (ICASSP 2014)*, pp. 1190–1194, IEEE Computer Society, Washington, DC (2014).
4. C. O. Ancuti et al., "A fast semi-inverse approach to detect and remove the haze from a single image," in *Asian Conf. on Computer Vision (ACCV 2010)*, pp. 501–514, Springer, Berlin Heidelberg (2010).
5. Y. Ting, L. J. Wang, and J. X. Wang, "Method to enhance degraded image in dust environment," *J. Software* **9**(10), 2672–2677 (2014).

Downloaded From: http://opticalengineering.spiedigitallibrary.org/ on 07/03/2017 Terms of Use: http://spiedigitallibrary.org/ss/termsofuse.aspx

6. R. Fattal, "Single image dehazing," *ACM Trans. Graph.* **27**(3), 1–9 (2008).
7. J. P. Tarel et al., "Improved visibility of road scene images under heterogeneous fog," in *Proc. IEEE Intelligent Vehicles Symp.*, pp. 478–485, IEEE Computer Society, Washington, DC (2010).
8. K. He, J. Sun, and X. Tang, "Single image haze removal using dark channel prior," *IEEE Trans. Pattern Anal. Mach. Intell.* **33**(12), 2341–2353 (2011).
9. Y. Y. Wang, Y. Z. Li, and T. X. Zhang, "Method to restore dust degraded images," *J. Huazhong Univ. Sci. Technol.* **38**(8), 42–45 (2010).
10. H. B. Li et al., "Removing dust impact for visual navigation in Mars landing," *J. Adv. Space Res.* **57**(1), 340–354 (2016).
11. J. Lu et al., "Real time defogging system used for video image of farmland based on modified dark channel prior algorithm," *Trans. Chin. Soc. Agric. Eng.* **32**(10), 143–148 (2016).
12. J. B. Wang et al., "Single image dehazing with a physical model and dark channel prior," *J. Neurocomput.* **149**, 718–728 (2015).
13. G. Meng et al., "Efficient image dehazing with boundary constraint and contextual regularization," in *Proc. IEEE Int. Conf. Computer Vision*, pp. 617–624, IEEE Computer Society, Washington, DC (2013).
14. Q. Zhu, J. Mai, and L. Shao, "A fast single image haze removal algorithm using color attenuation prior," *IEEE Trans. Image Process.* **24**(11), 3522–3533 (2015).
15. V. A. Kovalev and W. E. Eichinger, "Fundamentals of the LIDAR technique," in *Elastic Lidar: Theory, Practice, and Analysis Methods*, pp. 53–68, John Wiley & Sons, Inc., New York (2004).
16. Y. Li, G. P. Pan, and X. Wang, "Calculation of smoke transmission based on first-order multiple scattering approximation," *Chin. J. Explos. Propellants* **24**(2), 39–41 (2001).
17. J. E. Hansen, "Exact and approximate solutions for multiple scattering by cloudy and hazy planetary atmospheres," *J. Atmos. Sci.* **26**(3), 478–487 (1969).
18. J. H. Kim, J. Y. Sim, and C. S. Kim, "Single image dehazing based on contrast enhancement," in *Proc. IEEE Int. Conf. Acoustical, Speech, and Signal Processing*, pp. 1273–1276, IEEE Computer Society, Washington, DC (2011).
19. D. Park et al., "Single image dehazing with image entropy and information fidelity," in *Proc. IEEE Int. Conf. Image Processing*, pp. 4037–4041, IEEE Computer Society, Washington, DC (2014).
20. N. Baig et al., "Image dehazing using quadtree decomposition and entropy-based contextual regularization," *IEEE Signal Process. Lett.* **23**(6), 853–857 (2016).
21. K. He and J. Sun, "Fast guided filter," Technical Report, Computer Vision and Pattern Recognition (cs.CV), arXiv:1505.00996v1 (2015).
22. Z. Li et al., "Weighted guided image filtering," *IEEE Trans. Image Process.* **24**(1), 120–129 (2015).
23. A. Toet, "Alternating guided image filtering," *PeerJ Comput. Sci.* **2**, e72 (2016).
24. A. Polesel, G. Ramponi, and V. J. Mathews, "Image enhancement via adaptive unsharp masking," *IEEE Trans. Image Process.* **9**(3), 505–510 (2000).
25. N. Hautiere et al., "Blind contrast enhancement assessment by gradient ratioing at visible edges," *Image Anal. Stereol. J.* **27**(2), 87–95 (2008).
26. K. Ma, W. Liu, and Z. Wang, "Perceptual evaluation of single image dehazing algorithms," in *Image Processing (ICIP 2015)*, pp. 3600–3604, IEEE Computer Society, Washington, DC (2015).

Yuanyu Wang is a lecturer at Taiyuan University of Technology. He received his MS degree and PhD in mechatronics from Taiyuan University of Technology in 2003 and 2011, respectively. He is the author of more than 10 journal papers and has written four book chapters. His current research interests include computer vision and robot techniques.

Peter Yuen is a reader at Cranfield University leading a group on electro-optics, remote sensing, and computer vision research. He has about 75 journal and conference papers in the fields of semiconductor physics, computer vision, and defence science. He is a fellow of the Institute of Physics (FInstP) and the Institute of Mathematics and its Applications (FIMA) since 2001 and 2002, respectively.

Downloaded From: http://opticalengineering.spiedigitallibrary.org/ on 07/03/2017 Terms of Use: http://spiedigitallibrary.org/ss/termsofuse.aspx



https://dspace.org/

Image dehazing based on partitioning reconstruction and entropy-based alternating fast-weighted guided filters

Wang, Yuanyu; Yuen, Peter W. T.

2017-05-26

SPIE - International Society for Optics and Photonics

http://dx.doi.org/10.1117/1.OE.56.5.053111

Wang Y, Yuen P (2017) Image dehazing based on partitioning reconstruction and entropy-based alternating fast-weighted guided filters. Optical Engineering, Volume 56, Issue 5, May 2017, Article number 053111

Downloaded from a DSpace repository. https://dspace.org/